J|A|C|S
ARTICLES

Published on Web 12/18/2008

From Phenylsiloxane Polymer Composition to Size-Controlled Silicon Carbide Nanocrystals

Eric J. Henderson and Jonathan G. C. Veinot*

Department of Chemistry, University of Alberta, Edmonton, Alberta T6G 2G2, Canada

Received September 29, 2008; E-mail: jveinot@ualberta.ca

Abstract: Silicon carbide (SiC) has become a very important material for many high-performance applications as a result of its exceptional material properties. The emergence of size-dependent properties in SiC nanocrystals (SiC-NCs), together with the increased surface area intrinsic to nanocrystals, has led to a variety of new possible applications, including optoelectronics and hybrid materials. Here we report the straightforward preparation of size-controlled oxide-embedded and freestanding SiC-NCs from the reductive thermal processing of compositionally controlled phenylsiloxane polymers. Compositional tuning of the polymers is achieved by varying the relative amounts of phenyl trichlorosilane ($C_6H_5SiCl_3$) and silicon tetrachloride ($SiCl_4$) during hydrolysis and cocondensation. Thermal processing of the resulting compositionally controlled condensation copolymers yields oxide-embedded SiC-NCs whose average diameter is dependent on the relative $C_6H_5SiCl_3$ concentration in the initial precursor mixture. A liberation procedure for preparing size-controlled freestanding SiC-NCs that involves oxidation of matrix carbon and subsequent chemical etching of the matrix is also presented.

1. Introduction

Silicon carbide (SiC) is a very important material for many high-performance applications as a result of its exceptional electronic, physical, and chemical properties. Its wide band gap, high strength, thermal stability, and chemical inertness have led many to regard SiC as a promising substitute for silicon in high-power, high-temperature, high-frequency electronics.[1−6] These properties also make SiC ideal for integration into microelectromechanical systems (MEMS) for harsh-environment sensing applications.[7] As with many other materials, the current decades-long trend toward size reduction to nanoscale dimensions has led to a variety of new applications for SiC, arising from the emergence of size-dependent properties not found in the bulk material as well as the increased surface area, which leads to greater interfacial areas and interactions.

Similar to other Group IV semiconductor nanocrystals such as Si and Ge, SiC nanocrystals (SiC-NCs) have shown tremendous potential for optoelectronic applications as a result of their size-dependent optical and electronic properties.[1] The confinement of charge carriers in semiconductor nanocrystals and the resulting enhancement of the probability of radiative recombination, known as quantum confinement, is an effective method for tailoring photoluminescence (PL) properties in size-controlled nanocrystals. This strategy has been applied to Si and Ge nanocrystals that have exhibited PL maxima spanning the near-infrared (NIR) and visible spectrum.[8−10] Recently, similar successes in realizing control and increased stability of blue and UV PL from SiC-NCs[11−14] have demonstrated the potential for use of SiC in PL applications in this spectral regime, as these spectral regions are not easily accessed with Si-based systems. Furthermore, the stability of SiC-NC photoluminescence in aqueous media[15] together with its biocompatibility[16] make SiC-NCs ideal for biological fluorescence imaging.[17,18]

In addition to interest in the optical properties of SiC-NCs, the desirable physical properties of SiC, together with the large surface area intrinsic to nanocrystals, have also been exploited in hybrid materials for performance enhancement. The incor-

(1) Fan, J. Y.; Wu, X. L.; Chu, P. K. *Prog. Mater. Sci.* **2006**, *51*, 983–1031.
(2) Mélinon, P.; Masenelli, B.; Tournus, F.; Perez, A. *Nat. Mater.* **2007**, *6*, 479–490.
(3) Bhatnagar, M.; Baliga, B. J. *IEEE Trans. Electron Devices* **1993**, *40*, 645–655.
(4) Nakamura, D.; Gunjishima, I.; Yamaguchi, S.; Ito, T.; Okamoto, A.; Kondo, H.; Onda, S.; Takatori, K. *Nature* **2004**, *430*, 1009–1012.
(5) Willander, M.; Friesel, M.; Wahab, Q. U.; Straumal, B. *J. Mater. Sci.* **2006**, *17*, 1–25.
(6) Harris, C. I.; Savage, S.; Konstantinov, A.; Bakowski, M.; Ericsson, P. *Appl. Surf. Sci.* **2001**, *184*, 393–398.
(7) Mehregany, M.; Zorman, C. A.; Rajan, N.; Wu, C. H. *Proc. IEEE.* **1998**, *86*, 1594–1609.
(8) Hessel, C. M.; Henderson, E. J.; Veinot, J. G. C. *Chem. Mater.* **2006**, *18*, 6139–6146.
(9) Hessel, C. M.; Henderson, E. J.; Veinot, J. G. C. *J. Phys. Chem. C* **2007**, *111*, 6956–6961.
(10) Henderson, E. J.; Hessel, C. M.; Veinot, J. G. C. *J. Am. Chem. Soc.* **2008**, *130*, 3624–3632.
(11) Morales Rodriguez, M.; Díaz Cano, A.; Torchynska, T. V.; Polupan, G.; Ostapenko, S. *J. Non-Cryst. Solids* **2008**, *354*, 2272–2275.
(12) Rossi, A. M.; Murphy, T. E.; Reipa, V. *Appl. Phys. Lett.* **2008**, *92*, 253112.
(13) Wu, X. L.; Fan, J. Y.; Qiu, T.; Yang, X.; Siu, G. G.; Chu, P. K. *Phys. Rev. Lett.* **2005**, *94*, 026102.
(14) Fan, J. Y.; Wu, X. L.; Li, H. X.; Liu, H. W.; Siu, G. G.; Chu, P. K. *Appl. Phys. Lett.* **2006**, *88*, 041909.
(15) Fan, J. Y.; Wu, X. L.; Zhao, P. Q.; Chu, P. K. *Phys. Lett. A* **2006**, *360*, 336–338.
(16) Yakimova, R.; Petoral, R. M.; Yazdi, G. R.; Vahlberg, C.; Lloyd Spetz, A.; Uvdal, K. *J. Phys. D* **2007**, *40*, 6435–6442.
(17) Botsoa, J.; Lysenko, V.; Géloën, A.; Marty, O.; Bluet, J. M.; Guillot, G. *Appl. Phys. Lett.* **2008**, *92*, 173902.
(18) Fan, J.; Li, H.; Jiang, J.; So, L. K. Y.; Lam, Y. W.; Chu, P. K. *Small* **2008**, *4*, 1058–1062.

Scheme 1. Synthetic Outline for the Preparation of Size-Controlled SiC-NCs from Compositionally Controlled Phenylsiloxane Polymers[a]

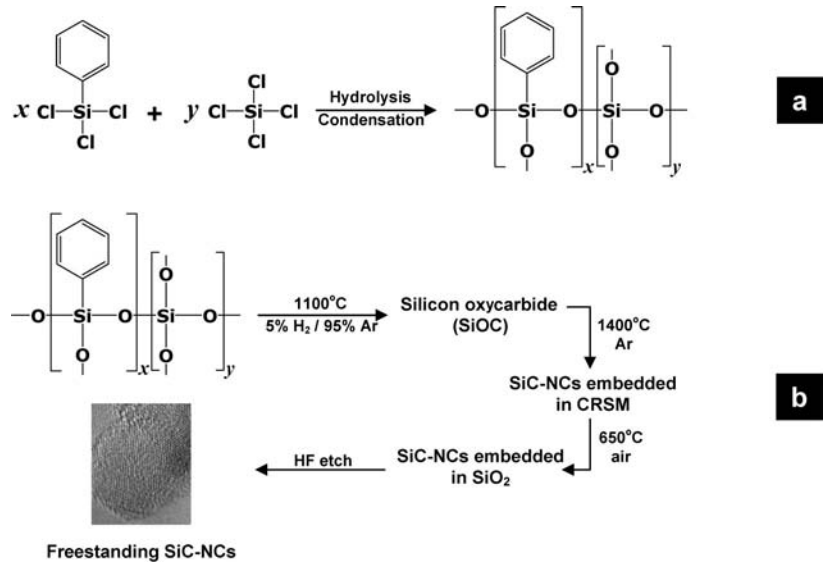

[a] (a) Hydrolysis and cocondensation of varying mixtures of $C_6H_5SiCl_3$ and $SiCl_4$ yields compositionally-controlled phenylsiloxane polymers, $[(C_6H_5SiO_{1.5})_x(SiO_2)_y]_n$. (b) Reductive thermal processing of $[(C_6H_5SiO_{1.5})_x(SiO_2)_y]_n$ polymers yields CRSM-embedded SiC-NCs. Subsequent oxidation of matrix carbon and chemical etching of the SiO_2 matrix yields freestanding size-controlled SiC-NCs.

poration of SiC-NCs into polymer films dramatically increases tensile strength and thermal stability[19,20] as a result of the efficient transfer of stress to the embedded nanocrystals. Furthermore, the stable, chemically inert, and large surface area of SiC nanostructures is ideal for heterogeneous catalyst supports.[21]

The most common approach for the preparation of SiC-NCs involves the electrochemical etching of bulk SiC wafers to yield porous SiC,[11] from which isolated nanocrystals can be obtained after grinding[17] or sonication.[1,12,13] These and other synthetic approaches, including ion implantation, thermal processing of C_{60}-loaded porous Si, and chemical vapor deposition, have recently been reviewed.[1]

For many applications, the production of size-selected nanocrystals is vital. The size dependence of the PL wavelength is well-established, with the consequence that specific nanocrystal sizes with small size polydispersity are required for narrow emission bands at the desired wavelength. It has also been shown that the Young's modulus and strength of particulate−polymer composites are strongly dependent on nanocrystal size below a diameter of ca. 20 nm,[22] further highlighting the importance of narrow size distributions. Ironically, the thermodynamic stability of SiC that gives rise to many of its desirable properties also imposes synthetic challenges for the production of size-controlled SiC-NCs. In particular, typical size-tuning approaches used for analogous Si-based systems, especially chemical etching, are not as accessible for SiC. Nevertheless, with a suitable synthetic approach, size control can be achieved in situ during nanocrystal formation and growth. This has been demonstrated with the formation of SiC-NCs from laser pyrolysis of gaseous mixtures[23] and from the electrochemical etching of SiC wafers.[1,13]

In this work, we report a new, straightforward, readily scalable method for the synthesis of size-controlled SiC-NCs via the thermal processing of compositionally controlled phenylsiloxane polymers. In brief, predetermined molar ratios of phenyl trichlorosilane ($C_6H_5SiCl_3$) and silicon tetrachloride ($SiCl_4$) were combined and polymerized by a standard sol−gel approach to produce phenylsiloxane polymers of tuned composition, $[(C_6H_5SiO_{1.5})_x(SiO_2)_y]_n$ (Scheme 1a). Controlled thermal processing of these polymers led to the formation of an amorphous silicon oxycarbide network, which underwent bond rearrangement to yield SiC-NCs embedded in a carbon-rich silica matrix (CRSM). Nanocrystal dimensions were found to depend directly upon the relative concentration of $C_6H_5SiCl_3$ in the initial polymerization mixture. A liberation procedure involving the thermal oxidation of matrix carbon followed by etching of the SiO_2 matrix has also been developed to effectively liberate size-controlled freestanding SiC-NCs (Scheme 1b).

2. Experimental Details

Reagents and Materials. Phenyl trichlorosilane (97%, Aldrich), silicon tetrachloride (99%, Aldrich), isopropyl alcohol (IPA, ≥99.5%, Fisher), electronic-grade hydrofluoric acid (HF, 49% aqueous solution, J. T. Baker), and reagent-grade ethanol (95%, Aldrich) were used as received. High-purity deionized (DI) water (18.2 MΩ/cm) was obtained from a Barnstead Nanopure Diamond purification system.

Preparation of $[(C_6H_5SiO_{1.5})_x(SiO_2)_y]_n$ Polymers (A1, B1, C1). In a typical synthesis, predetermined amounts of $C_6H_5SiCl_3$ and $SiCl_4$ were combined and magnetically stirred under an inert Ar atmosphere for 1 h in a salt water/ice bath (ca. −10 °C). The $C_6H_5SiCl_3/SiCl_4$ molar ratio was adjusted for each sample to obtain polymers of different compositions (Table 1). A 65% (v/v) solution of IPA in DI water was injected through a septum into the cooled mixture with vigorous stirring, using standard Schlenk techniques. IPA was added to the reaction solution to control the condensation reactions by simultaneously decreasing the water concentration and the hydrolysis rates through the formation of alkoxy-substituted

(19) Guo, Z.; Kim, T. Y.; Lei, K.; Pereira, T.; Sugar, J. G.; Hahn, H. T. *Compos. Sci. Technol.* **2008**, *68*, 164–170.
(20) Rodgers, R. M.; Mahfuz, H.; Rangari, V. K.; Chisholm, N.; Jeelani, S. *Macromol. Mater. Eng.* **2005**, *290*, 423–429.
(21) Ledoux, M. J.; Pham-Huu, C. *CATTECH* **2001**, *5*, 226–246.
(22) Fu, S.-Y.; Feng, X.-Q.; Lauke, B.; Mai, Y.-W. *Composites, Part B* **2008**, *39*, 933–961.
(23) Herlin-Boime, N.; Vicens, J.; Dufour, C.; Ténégal, F.; Reynaud, C.; Rizk, R. *J. Nanopart. Res.* **2004**, *6*, 63–70.

Table 1. Experimental Details for the Preparation of Compositionally Controlled $[(C_6H_5SiO_{1.5})_x(SiO_2)_y]_n$ Polymers from the Hydrolysis and Condensation of Phenyl Trichlorosilane ($C_6H_5SiCl_3$) and Silicon Tetrachloride ($SiCl_4$)

sample	$C_6H_5SiCl_3/SiCl_4$ molar ratio	$V_{C_6H_5SiCl_3}$ (mL)[a]	V_{SiCl_4} (mL)[b]	$V_{65\%\ IPA}$ (mL)
A1	1:1	2.8	2.0	16.0
B1	1:1.5	2.8	3.0	20.5
C1	1:2	2.8	4.0	25.0

[a] Each 2.8 mL aliquot contained 17.5 mmol of $C_6H_5SiCl_3$. [b] The aliquots for **A1**, **B1**, and **C1** contained 17.5, 26.3, and 35.0 mmol of $SiCl_4$, respectively.

Table 2. Sample List and Experimental Details for the Preparation of Liberated SiC-NCs from Compositionally Controlled $[(C_6H_5SiO_{1.5})_x(SiO_2)_y]_n$ Polymers

sample	precursor, processing conditions	remarks
A2	**A1**, 1100 °C, 1 h, 5% H_2/95% Ar	amorphous oxycarbide network
B2	**B1**, 1100 °C, 1 h, 5% H_2/95% Ar	amorphous oxycarbide network
C2	**C1**, 1100 °C, 1 h, 5% H_2/95% Ar	amorphous oxycarbide network
A3	**A2**, 1400 °C, 2 h, Ar	SiC-NCs in CRSM
B3	**B2**, 1400 °C, 2 h, Ar	SiC-NCs in CRSM
C3	**C2**, 1400 °C, 2 h, Ar	SiC-NCs in CRSM
A4	**A3**, 650 °C, 30 min, air	SiC-NCs in SiO_2 matrix
B4	**B3**, 650 °C, 30 min, air	SiC-NCs in SiO_2 matrix
C4	**C3**, 650 °C, 30 min, air	SiC-NCs in SiO_2 matrix
A5	**A4**, HF etching, 1 h	liberated SiC-NCs
B5	**B4**, HF etching, 1 h	liberated SiC-NCs
C5	**C4**, HF etching, 1 h	liberated SiC-NCs

intermediates. The volume of aqueous solution added to the mixture was adjusted for each sample to maintain a constant H_2O/Cl ratio for each polymer composition. As the reaction produces HCl (g), an exhaust vent was connected to the reaction flask to prevent overpressurization. The clear, colorless mixture of $C_6H_5SiCl_3$ and $SiCl_4$ immediately turned cloudy white as the IPA solution was added, and hydrolysis of the precursors was confirmed by monitoring the pH of the reaction mixture (pH 1). The cloudy white mixture was stirred for 24 h at ambient temperature and subsequently for 3 h at 70 °C to promote further condensation. The resulting white solid precipitate was isolated by vacuum filtration, washed 3× with DI water, and dried in vacuo. The white solid polymers **A1**, **B1**, and **C1** were obtained in yields greater than 90% and are stable under ambient conditions.

Preparation of Bulk Oxide-Embedded SiC-NCs (A2−A4, B2−B4, C2−C4). $[(C_6H_5SiO_{1.5})_x(SiO_2)_y]_n$ polymer (**A1**, **B1**, or **C1**) was placed in a quartz reaction boat and transferred to a high-temperature tube furnace. Each sample was thermally processed at 1100 °C for 1 h under a slightly reducing atmosphere (5% H_2/95% Ar). The resulting glassy black silicon oxycarbide (**A2**, **B2**, or **C2**) was subsequently transferred to a vitreous carbon reaction boat and thermally processed at 1400 °C for 2 h under an inert Ar atmosphere to produce the corresponding SiC-NCs embedded in a CRSM (**A3**, **B3**, or **C3**). A final thermal processing step involved heating the solid in air at 650 °C for 30 min to produce SiO_2-embedded SiC-NCs (**A4**, **B4**, or **C4**). After the sample was cooled to room temperature, the solid composite was mechanically ground in an agate mortar and pestle. Details of these procedures are summarized in Table 2.

Liberation of Freestanding SiC-NCs (A5, B5, C5). Freestanding SiC-NCs were liberated from the oxide by chemical etching of the SiO_2 matrix in a HF solution. In a typical liberation procedure, 0.05 g of **A4**, **B4**, or **C4** was magnetically stirred in 3 mL of a 1:1:1 DI water/ethanol/49% HF solution for 1 h (Table 2). The corresponding freestanding SiC-NCs **A5**, **B5**, or **C5** were isolated by centrifugation, washed with DI water and ethanol, and dried under a flowing stream of Ar.

Fourier Transform Infrared Spectroscopy (FTIR). FTIR spectroscopy of free-flowing powders of **A1−A5**, **B1−B5**, and **C1−C5** was performed using a Nicolet Magna 750 IR spectrophotometer.

X-ray Powder Diffraction (XRD). XRD was performed using an INEL XRG 3000 X-ray diffractometer equipped with a Cu Kα radiation source (λ = 1.54 Å). Bulk crystallinity for samples **A2−A5**, **B2−B5**, and **C2−C5** was evaluated on finely ground samples mounted on a low-intensity-background silicon (100) sample holder.

X-ray Photoelectron Spectroscopy (XPS). XPS analysis was performed using a Kratos Axis Ultra instrument operating in energy-spectrum mode at 210 W. The base pressure and operating chamber pressure were maintained at $\leq 10^{-7}$ Pa. A monochromatic Al Kα source (λ = 8.34 Å) was used to irradiate the samples, and the spectra were obtained with an electron takeoff angle of 90°. To control sample charging, the charge neutralizer filament was used when required. Survey spectra were collected using an elliptical spot with major and minor axis lengths of 2 and 1 mm, respectively, and a 160 eV pass energy with a step of 0.33 eV. CasaXPS software (Vamas) was used to process high-resolution (HR) spectra. All of the spectra were internally calibrated to the O 1s emission (532.9 eV). After calibration, the background from each spectrum was subtracted using a Shirley-type background to remove most of the extrinsic loss structure.

Transmission Electron Microscopy (TEM). High-resolution TEM (HRTEM) was performed at the Brockhouse Institute for Materials Research (BIMR) at McMaster University using a JEOL-2010 field-emission gun operating at 200 keV. Low-resolution TEM was performed using a JEOL-2010 electron microscope with a LaB_6 thermionic emission source operating at 200 keV. TEM samples of freestanding SiC-NCs (**A5**, **B5**, **C5**) were drop-coated from an ethanol suspension onto a carbon-coated copper grid.

3. Results and Discussion

Polymer Composition. The effect of the phenylsiloxane polymer composition (i.e., the $C_6H_5SiO_{1.5}/SiO_2$ ratio) on the SiC-NC diameter was monitored by synthesizing three polymers of decreasing phenyl concentration having $C_6H_5SiCl_3/SiCl_4$ molar ratios of 1:1 (**A1**), 1:1.5 (**B1**), and 1:2 (**C1**) (Table 1). The formation of phenylsiloxanes was confirmed by FTIR spectroscopy (Figure 1a). FTIR spectra of all three polymers show characteristic aromatic C−H stretching at 3100−3000 cm^{-1}, aromatic C═C stretching at 1430 and 1595 cm^{-1}, C−H bending at ca. 695 and 740 cm^{-1}, and intense Si−O−Si stretching modes at ca. 1150 cm^{-1}, supporting the formation of phenyl-containing siloxane species, consistent with the proposed hydrolyzed/condensed structures and previous investigations on phenylsiloxanes.[24] The appearance of a broad O−H stretch centered at ca. 3400 cm^{-1} likely arises from uncondensed Si−OH groups, consistent with the absorptions at 3635 and 3740 cm^{-1} from H-bonded and isolated silanols, respectively.[25]

XPS was performed to further elucidate the composition of the phenylsiloxane polymers by monitoring the Si coordination environments. The Si 2p region of the XP spectra for the three polymers **A1**, **B1**, and **C1** shows a broad emission centered at 103.2 eV (Figure 1b) that is readily fit to contributions arising from "$Si(C_6H_5)O_3$" and "SiO_4" species, with Si $2p_{3/2}$ components centered at 102.7 and 103.4 eV, respectively. These are in agreement with reported binding energies for phenylsilicone

(24) Hurwitz, F. I.; Heimann, P.; Farmer, S. C.; Hembree, D. M., Jr. *J. Mater. Sci.* **1993**, *28*, 6622–6630.
(25) Van Le, T.; Ross, E. E.; Velarde, T. R. C.; Legg, M. A.; Wirth, M. J. *Langmuir* **2007**, *23*, 8554–8559.

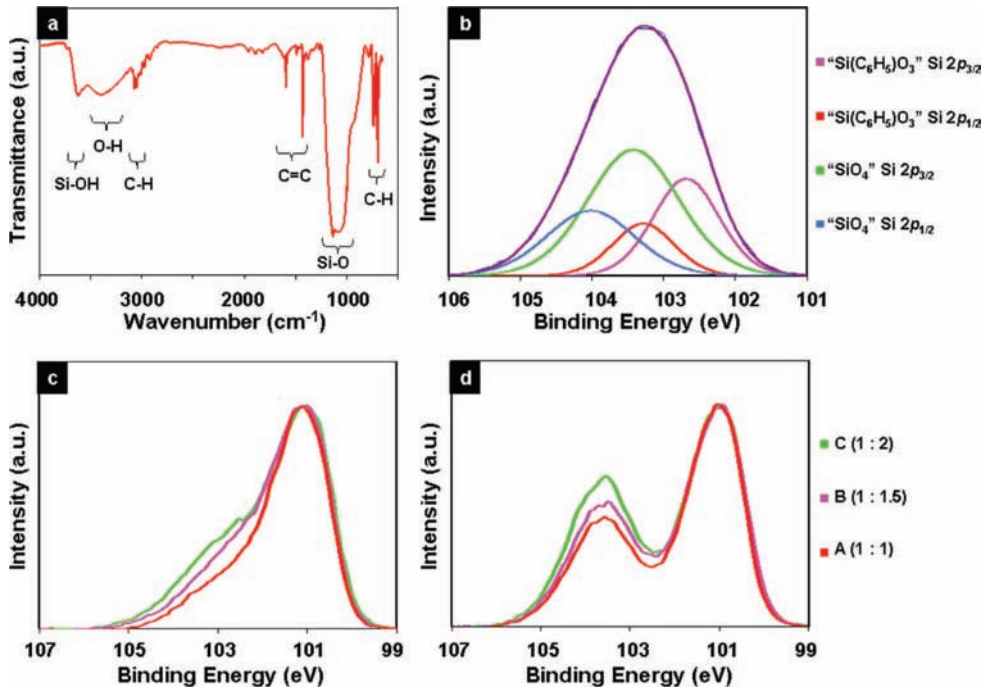

Figure 1. Spectroscopic characterization of phenylsiloxane polymers and oxide-embedded SiC-NCs. (a) FTIR spectrum of polymer **C1** showing characteristic absorptions of phenylsiloxanes. (b) HR XP spectrum of the Si 2p region of polymer **C1** fit to $2p_{3/2}$ and $2p_{1/2}$ spin−orbit partner lines of "$C_6H_5SiO_3$" and "SiO_4" components, consistent with compositionally tailored phenylsiloxane. (c) HR XP spectra of the Si 2p region of CRMS-embedded SiC-NCs **A3**, **B3**, and **C3**. (d) HR XP spectra of the Si 2p region of SiO_2-embedded SiC-NCs **A4**, **B4**, and **C4**. (c) and (d) clearly show the relationship between polymer and composite compositions.

resin $[(C_6H_5SiO_{1.5})_n]$ and SiO_2[26] and support the presented FT-IR analysis of the formation of $[(C_6H_5SiO_{1.5})_x(SiO_2)_y]_n$ condensation polymers.

In order to confirm that varying the monomer ratios in the initial polymerization mixture led to compositional tuning of the polymers, relative changes in the Si coordination environments were monitored by XPS for the matrix-embedded SiC-NCs produced from reductive thermal processing of each of the polymers. The Si 2p regions of the XP spectra of CRSM-embedded SiC-NCs **A3**, **B3**, and **C3** (Figure 1c) and the SiO_2-embedded SiC-NCs **A4**, **B4**, and **C4** (Figure 1d) are dominated by a feature centered at 101 eV arising from the SiC-NCs.[27] When the spectra were normalized to this SiC feature, the relative intensity of the emission from silicon oxide species, 103−105 eV, clearly increases with $SiCl_4$ concentration in the initial polymerization mixture, with the greatest intensity observed for **C3** and **C4**. These results establish that **C1** had the greatest incorporation of SiO_2, a direct result of the tailored polymer composition.

Size Control of Oxide-Embedded SiC-NCs. The effect of precursor polymer composition on the average diameter of oxide-embedded SiC-NCs was evaluated by XRD. The powder diffraction patterns of the CRSM-embedded SiC-NCs **A3**, **B3**, and **C3** (Figure 2a) are characterized by broad reflections centered at 36, 60, and 72° that are readily indexed to the (111), (220), and (311) crystal planes of β-SiC, respectively.[28] From this, it is apparent that broadening of the reflections from SiC-NCs increases as the polymer phenyl concentration decreases (i.e., in going from **A3** to **C3**). This trend is clearly evident in the evaluation of the (220) reflection (Figure 2b). An estimate of particle size was obtained using Scherrer analysis of the XRD peak broadening, which provided mean SiC-NC diameters of ca. 9, 7, and 5 nm for **A3**, **B3**, and **C3**, respectively. Clearly, the size of SiC-NCs produced by this method is effectively controlled by the phenylsiloxane polymer composition. This trend is also clearly evident in the TEM analysis of liberated SiC-NCs (see below).

Matrix Liberation of SiC-NCs. Many potential applications of SiC-NCs require freestanding particles, and therefore, an oxide liberation procedure involving the thermal oxidation of graphitic carbon in the CRSM followed by HF etching of SiO_2 was developed. It is known that SiC is thermally stable and unaffected by HF under the present conditions,[29] and thus, this liberation procedure did not compromise the SiC crystallinity or result in any detectable change in the SiC-NC dimensions. The Si 2p region of the XP spectrum of liberated SiC-NCs **C5** (Figure 3a) is dominated by an emission centered at 101 eV, consistent with SiC.[27] After the spectrum was fit to the Si $2p_{3/2}$ and $2p_{1/2}$ spin−orbit partner lines, a low-intensity shoulder remained on the high energy side of this feature, centered at 102.6 eV. We attribute this component to mixed surface species arising from the HF etching procedure and postetching oxidation (see below).

Electrochemical etching of SiC in aqueous HF solutions has been shown to result in complex surface chemistry, including oxide, hydroxide, fluoride, and hydride species.[30−32] The FTIR spectrum of liberated SiC-NCs **C5** (Figure 3b) clearly shows the dominant SiC transverse optical phonon (TOP) vibration[27]

(26) Wagner, C. D.; Passoja, D. E.; Hillery, H. F.; Kinisky, T. G.; Six, H. A.; Jansen, W. T.; Taylor, J. A. *J. Vac. Sci. Technol.* **1982**, *21*, 933–944.
(27) Avila, A.; Montero, I.; Galán, L.; Ripalda, J. M.; Levy, R. *J. Appl. Phys.* **2001**, *89*, 212–216.
(28) Yang, W.; Miao, H.; Xie, Z.; Zhang, L.; An, L. *Chem. Phys. Lett.* **2004**, *383*, 441–444.
(29) Zhuang, D.; Edgar, J. H. *Mater. Sci. Eng., R* **2005**, *48*, 1–46.

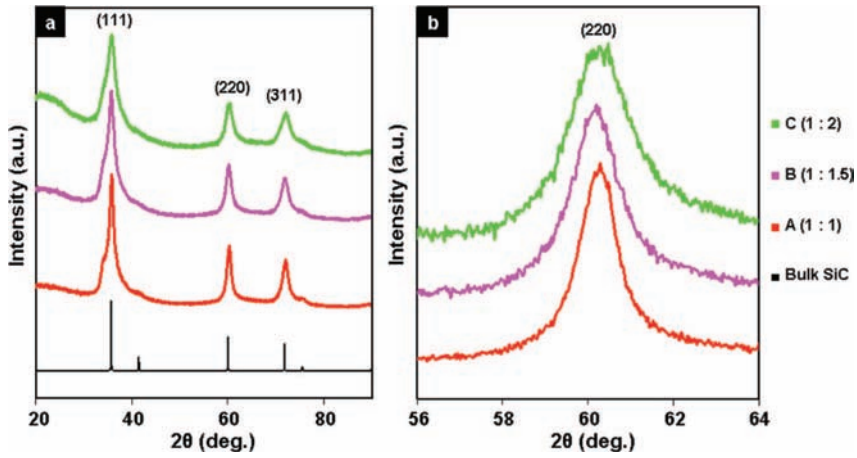

Figure 2. XRD characterization of oxide-embedded SiC-NCs and evidence for size tunability based on phenylsiloxane composition. (a) XRD patterns of CRSM-embedded SiC-NCs **A3**, **B3**, and **C3** showing reflections characteristic of β-SiC. (b) XRD patterns highlighting the (220) reflections of CRSM-embedded SiC-NCs **A3**, **B3**, and **C3** that clearly show crystal-size control as a result of compositionally tailored polymers.

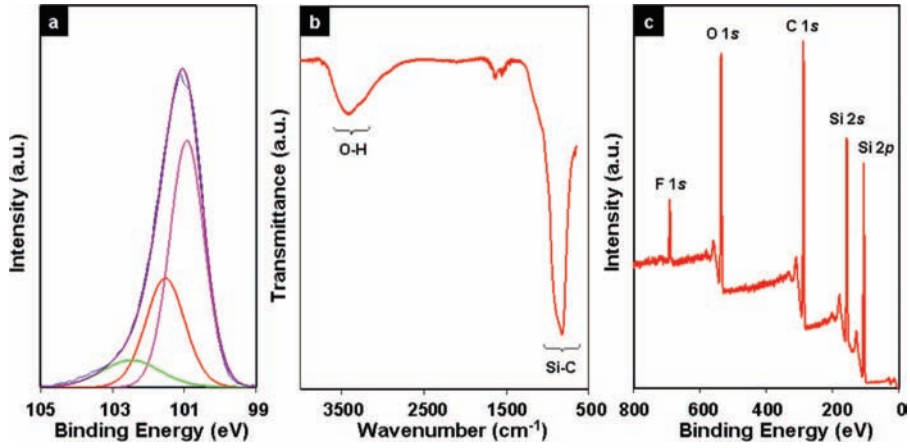

Figure 3. Spectroscopic characterization of freestanding SiC-NCs. (a) HR XP spectrum of the Si 2p region of freestanding SiC-NCs **C5** fit to the $2p_{3/2}$ (magenta) and $2p_{1/2}$ (red) spin−orbit partner lines of SiC and a high-energy component (green) attributed to surface oxide, hydroxide, and fluoride species. (b) FTIR spectrum of freestanding SiC-NCs **C5**, showing the Si−C TOP vibration and an O−H stretch attributed to surface hydroxides. (c) XP survey spectrum of freestanding SiC-NCs **C5**, showing the presence of fluoride and oxide species.

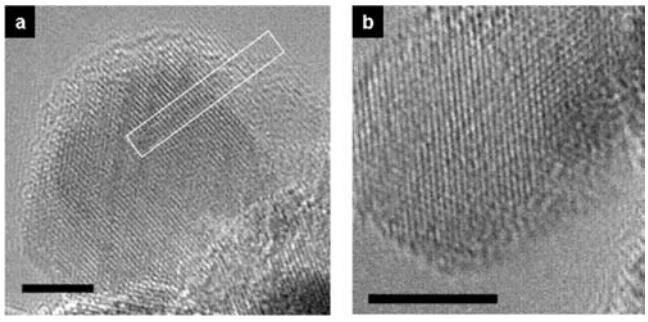

Figure 4. HRTEM of freestanding SiC-NCs. (a) HRTEM image of liberated SiC-NCs **A5** with a measured diameter of ca. 10 nm, showing lattice fringes consistent with crystalline β-SiC. The enclosed area was used to calculate the average crystal lattice spacing (2.5 Å). (b) HRTEM image of liberated SiC-NCs **C5** with a measured diameter of ca. 6 nm, also showing lattice fringes consistent with crystalline β-SiC. Both scale bars represent 5 nm.

centered at 835 cm^{-1}, a broad O−H stretch centered at ca. 3400 cm^{-1}, and a shoulder at ca. 1100 cm^{-1} from Si−O species. It is unlikely that this low-intensity feature arises from incomplete etching of the oxide matrix; instead, it is probably due to species produced by postetching surface oxidation. In this regard, it is reasonable that surface Si−H species oxidize during the postetching workup. The presence of fluorine in the XP survey spectrum of the liberated SiC-NCs (Figure 3c) also suggests partial fluoride surface termination as a result of HF treatment. These results indicate that the present liberated SiC-NCs possess complex surface chemistry. To effectively interface the nanocrystals with application-specific environments (e.g., polymer matrices or aqueous biological systems), a detailed understanding of, and ability to control, the SiC-NC surface chemistry is desirable. This is the subject of ongoing study in our laboratory. A hydroxylated SiC crystal surface is one candidate currently being explored that has already proven to be a useful platform for subsequent chemical derivitization for bulk systems.[30,31]

The SiC-NC size control achieved through variations in polymer composition can be directly observed by examining the HRTEM images of the liberated nanocrystals **A5** and **C5** (Figure 4a,b). It is clear that the diameters of the pseudospherical nanocrystals differ significantly, with measured sizes of ca. 10 and 6 nm for **A5** and **C5**, respectively. The measured crystal

(30) Rosso, M.; Arafat, A.; Schroën, K.; Giesbers, M.; Roper, C. S.; Maboudian, R.; Zuilhof, H. *Langmuir* **2008**, *24*, 4007–4012.
(31) Schoell, S. J.; Hoeb, M.; Sharp, I. D.; Steins, W.; Eickhoff, M.; Stutzmann, M.; Brandt, M. S. *Appl. Phys. Lett.* **2008**, *92*, 153301.
(32) Alekseev, S. A.; Zaitsev, V. N.; Botsoa, J.; Barbier, D. *Chem. Mater.* **2007**, *19*, 2189–2194.

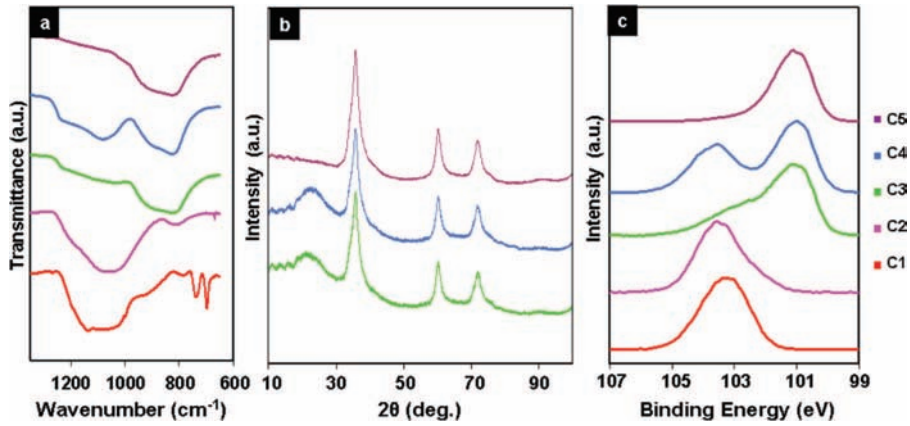

Figure 5. Characterization of the mechanism of SiC-NC formation from phenylsiloxane polymers and subsequent oxide liberation: evolution of (a) FTIR spectra, (b) XRD patterns, and (c) HR XP spectra of the Si 2p region for the 1:2 $C_6H_5SiCl_3/SiCl_4$ (**C**) system through various stages in the formation and liberation of SiC-NCs.

lattice spacing for both samples (2.5 Å) was readily indexed to the (111) crystal plane of β-SiC. The presence of a noncrystalline shell surrounding the crystalline core of the SiC-NCs is consistent with the formation of an amorphous surface species that results from etching and subsequent oxidation. Size distributions for **A5**, **B5**, and **C5** were obtained from low-resolution TEM images (Figures 1−3 in the Supporting Information) and determined to be 8.9 nm ($n = 150$, $\sigma = 1.1$ nm), 6.8 nm ($n = 150$, $\sigma = 1.0$ nm), and 5.5 nm ($n = 150$, $\sigma = 0.8$ nm), respectively. These measured values are in excellent agreement with the XRD size analysis (see above) and highlight the narrow size distributions obtained through this method.

Thermal Transformation Pathway. The mechanism that leads to SiC-NC formation from the thermal processing of our phenylsiloxane polymers was investigated by following the evolution of the XRD patterns and FTIR and XP spectra for the 1:2 $C_6H_5SiCl_3/SiCl_4$ (**C**) system. For clarity, we present this evolution in five stages:

(1) As previously mentioned, the FTIR spectrum (Figure 5a) of the unprocessed polymer **C1** is dominated by Si−O−Si stretching centered at ca. 1150 cm^{-1} and characteristic phenyl vibrational modes. The XP spectrum (Figure 5c) shows a single broad emission centered at ca. 103 eV that can be fit to Si species made up of Si tetrahedrally bonded to four oxygen atoms (103.4 eV) and to three oxygen atoms and one sp^2-hybridized carbon (102.7 eV), consistent with a $[(C_6H_5SiO_{1.5})_x(SiO_2)_y]_n$ composition.

(2) Thermal processing at 1100 °C in a slightly reducing atmosphere (5% H_2/95% Ar) to give **C2** is accompanied by a decrease and eventual loss of all IR absorptions associated with phenyl functionalities and a broadening of the Si−O−Si stretching mode (Figure 5a). Similar observations have been reported for pyrolysis of polyphenylsilsesquioxane and have been attributed to thermal decomposition of phenyl groups and a breakdown of the well-defined Si−O−Si backbone structure into a disorganized extended silicon oxycarbide network.[33] At this stage of the present synthesis, the XRD pattern (Figure 5b) shows no evidence of crystalline phases. The XP spectrum (Figure 5c) shows a broadening of the Si 2p spectral feature and a slight shift to higher binding energies, attributed to the array of tetrahedrally bonded silicon species present in the oxycarbide network.

(3) Increasing the processing temperature to 1400 °C in an inert Ar atmosphere to give **C3** leads to the emergence of an absorption centered at ca. 835 cm^{-1} in the FTIR spectrum (Figure 5a) that is characteristic of the TOP vibration in SiC.[27] A low-intensity Si−O−Si absorption band arising from silicon oxide species in the matrix is also observed. The XRD pattern (Figure 5b) shows broad reflections centered at ca. 36, 60, and 72° that are readily indexed to the (111), (220), and (311) crystal planes of β-SiC, respectively. A broad spectral feature centered at ca. 20° characteristic of amorphous SiO_2 is also observed. The emergence of an intense feature centered at ca. 101 eV in the XP spectrum (Figure 5c) is consistent with the formation and phase segregation of crystalline SiC, while the broad high-energy shoulder is attributed to silicon oxide in the matrix.

(4) Thermal processing at 650 °C in air to produce **C4** causes a relative increase in intensity of the Si−O−Si absorption band in the FTIR spectrum (Figure 5a) that arises from the simultaneous oxidation of graphitic carbon in the matrix, which is evolved as CO_2, and a transformation of the matrix to amorphous SiO_2. Heating in air does not alter the SiC-NC diameter, as evidenced by the unchanged breadth of the XRD reflections (Figure 5b). We also note an increase in the intensities of the features assigned to amorphous SiO_2 in the XRD pattern and the XP spectrum (Figure 5c).

(5) Liberation of freestanding SiC-NCs **C5** through HF etching of the SiO_2 matrix is characterized by a nearly complete loss of the Si−O−Si band in the FTIR spectrum (Figure 5a). A low-intensity shoulder at ca. 1100 cm^{-1} is attributed to slight surface oxidation. As expected, chemical etching of SiO_2 is accompanied by the loss of the feature at ca. 20° in the XRD pattern (Figure 5b) and the SiO_2 spectral feature at 103.4 eV in the XP spectrum (Figure 5c).

Our results agree with the accepted mechanisms describing the thermally induced transformations leading to the formation of SiC from polyorganosiloxanes (i.e., sequential decomposition, bond rearrangement, and phase segregation). Initial pyrolytic decomposition of organic fragments up to temperatures of 1000−1200 °C produces an amorphous silicon oxycarbide (SiOC) network consisting of sp^3-hybridized carbon[24] and all

possible forms of tetrahedrally bonded silicon (SiC_4, SiC_3O, SiC_2O_2, $SiCO_3$, and SiO_4) (eq 1).[34]

$$\begin{aligned} 2RSiO_{1.5} &\rightarrow R_2SiO + SiO_2 \\ R_2SiO + RSiO_{1.5} &\rightarrow R_3SiO_{0.5} + SiO_2 \\ R_3SiO_{0.5} + RSiO_{1.5} &\rightarrow R_4Si + SiO_2 \end{aligned} \quad (1)$$

Subsequent thermal processing up to 1400 °C induces continued bonding rearrangement, leading to phase segregation of crystalline SiC, amorphous SiO_2, and disordered graphitic (sp^2) carbon.[24,34] This process is driven by the thermodynamic stability of SiC and SiO_2. It should be noted that in this temperature range (≤1400 °C), carbothermal reduction is not the primary pathway in the production of SiC. While formation of crystalline SiC *nanodomains* through these reactions has been identified,[24] this transformation has not been exploited until now for the production of either matrix-embedded or freestanding size-controlled SiC-NCs.

Ceramic prepolymers, such as polyorganosiloxanes (or polysilsesquioxanes)[24,33,34] and polycarbosilanes,[35−37] have been extensively studied as precursors to SiC. Their ease of synthesis, compositional versatility, thermal and oxidative stability, and solution processability make them attractive.[34] Among these many possible polymers, phenylsiloxanes are very appealing as SiC precursors because unsaturated organic groups bonded to silicon are less likely to be cleaved upon pyrolysis.[34] In fact, in studies performed on copolymers from phenyl and methyl trimethoxysilanes, it was found that the carbon content in the oxycarbide phase increased with phenyl concentration in the copolymer, leading to an increase in the amount of SiC.[24,37] Clearly, controlling the amount of carbon available in the amorphous SiOC network through phenyl content provides a direct pathway for influencing the formation and growth of crystalline SiC. Furthermore, by diluting the silicon and carbon with additional matrix elements (e.g., SiO_2) on a molecular scale, the bond rearrangements and solid-state diffusion processes leading to phase segregation can generate smaller crystalline domains of SiC. We have successfully demonstrated this strategy by copolymerizing a "matrix SiO_2"-generating monomer ($SiCl_4$) and a "SiC"-generating monomer ($PhSiCl_3$). By varying the relative concentrations of these monomers during polymerization, polymers of controlled composition were produced, leading to composites of tailored carbon concentrations and ultimately to size-controlled SiC-NCs. In short, increased carbon content in the parent polymer leads to larger SiC-NCs. We also developed a liberation procedure for producing freestanding size-controlled SiC-NCs. The freestanding SiC-NCs described in this contribution did not exhibit PL, as a result of a combination of factors including complex surface chemistry and the relatively large crystal size.[1] We are currently extending our investigation to produce smaller-diameter nanocrystals in order to probe their light-emission properties. Because of the straightforward nature of the present procedure and the size control achievable through this approach, we believe that this method will significantly contribute to current endeavors aimed at incorporating size-controlled SiC-NCs into device applications.

Acknowledgment. The authors acknowledge funding from the Natural Sciences and Engineering Research Council of Canada (NSERC), the Canada Foundation for Innovation (CFI), the Alberta Science and Research Investment Program (ASRIP), and the University of Alberta Department of Chemistry. C.W. Moffat and R. Lister are thanked for assistance with FTIR spectroscopy. The staff of the Alberta Centre for Surface Engineering and Sciences (ACSES) are thanked for XPS analysis. Carmen Andrei and the Brockhouse Institute for Materials Research are thanked for HRTEM imaging. J. Kelly, D. Rollings, S. McFarlane, Dr. C. Hessel, J. Rodriguez, M. Dang, R. Chisholm, and T. Telesco are also thanked for useful discussions.

Supporting Information Available: Low-resolution TEM images and size distributions of freestanding SiC-NCs. This material is available free of charge via the Internet at http://pubs.acs.org.

JA807701Y

(33) Ma, J.; Shi, L. H.; Zhang, J. M.; Li, B. Y.; Shen, D. Y.; Xu, J. *Chin. J. Polym. Sci.* **2002**, *20*, 573–577.
(34) Burns, G. T.; Taylor, R. B.; Xu, Y.; Zangvil, A.; Zank, G. A. *Chem. Mater.* **1992**, *4*, 1313–1323.
(35) Liu, Q.; Wu, H. J.; Lewis, R.; Maciel, G. E.; Interrante, L. V. *Chem. Mater.* **1999**, *11*, 2038–2048.
(36) Boury, B.; Corriu, R. J. P.; Douglas, W. E. *Chem. Mater.* **1991**, *3*, 487–489.
(37) Monthioux, M.; Delverdier, O. *J. Eur. Ceram. Soc.* **1996**, *16*, 721–737.